Chemistry of Sulfur Oxides on Transition Metals. III. Oxidation of SO_2 and Self-Diffusion of O, SO_2, and SO_3 on Pt(111)

Xi Lin

Department of Chemistry, Massachusetts Institute of Technology, Cambridge, Massachusetts 02139-4301

William F. Schneider

Physical and Environmental Sciences Department, Ford Research Laboratory, MD 3083-SRL, Dearborn, Michigan 48121-2053

Bernhardt L. Trout*

Department of Chemical Engineering, Massachusetts Institute of Technology, Cambridge, Massachusetts 02139-4301

Received: April 5, 2004; In Final Form: June 14, 2004

The chemical kinetics of the Pt catalyzed oxidation reaction $SO_2(g) + {}^1/_2O_2(g) \overset{Pt}{\leftrightarrow} SO_3(g)$ are studied using first-principles density functional theory (DFT). The diffusion processes of O, SO_2, and SO_3 are investigated in detail, revealing complex and unintuitive behavior. It is found that the self-diffusivities decrease in the order SO_2, O, and SO_3. For the formation of SO_3, both the Langmuir−Hinshelwood and the Eley−Rideal surface reaction steps are investigated in p(2×2) supercells, and the activation energies are found to be 46 and 25 kJ/mol, respectively. Both of these activation energies are much smaller than the SO_3 desorption energy of 113 kJ/mol.

I. Introduction

Understanding the chemical kinetics of surface reactions plays a key role in designing and improving the efficiency of heterogeneous catalysts. Tremendous experimental progress has been achieved by the development of state-of-art techniques, such as molecular beams, state-specific probing lasers, scanning tunneling microscopes, and quasi-elastic Helium atom scattering.[1−3] Complementary to these experimental techniques, detailed descriptions of chemical kinetics at the molecular level from theoretical point of view have become possible only recently owing to the development of modern first-principles quantum mechanical computations.[4,5]

Pt metal has long been known to be an effective SO_2 oxidation and reduction catalyst. Interest in the chemistry of sulfur oxides on transition metal surfaces increased with the introduction of the automotive three-way catalyst (composed of Pt, Rh, and Pd supported on high surface area alumina) in the late 1970s and the need to control their activity for formation and release of odorous H_2S.[6−8] The addition of basic oxides, like baria, into three-way catalyst formulations enables them to store nitrogen oxides (NO_x) under oxidizing conditions and thus to be useful as "lean NO_x traps." Unfortunately, the same Pt-catalyzed oxidation and baria-based adsorption chemistry that underlies NO_x storage also operate on the sulfur oxides, so that NO_x storage activity is readily poisoned by the more strongly adsorbing SO_x. A better understanding of sulfur oxidation on Pt catalysts will provide useful insight into aid in the development of more sulfur-tolerant lean-NO_x traps.[9]

Experimentally, identification of stable surface-bound sulfur oxide species is difficult due to the underlying sensitivity to both coverages and surface temperatures.[8] First-principles computations have been demonstrated to be an efficient approach to determining the thermodynamics of sulfur oxides on transition metals such as Cu[10] and Pt.[11] The thermodynamics of sulfur oxide surface species (SO_x, $x = 0$, 1, 2, 3, and 4) as a function of coverage on the Pt(111) single-crystal surface at low and intermediate temperatures have been produced via first-principles DFT computations.[12] These calculations show that, in the limit of low surface coverage, adsorbed sulfur oxides are thermodynamically unstable with respect to dissociation to adsorbed atomic S and O. At high surface O coverage, as might be expected to be present under highly oxidizing reaction conditions, oxidation to the higher sulfur oxides is instead

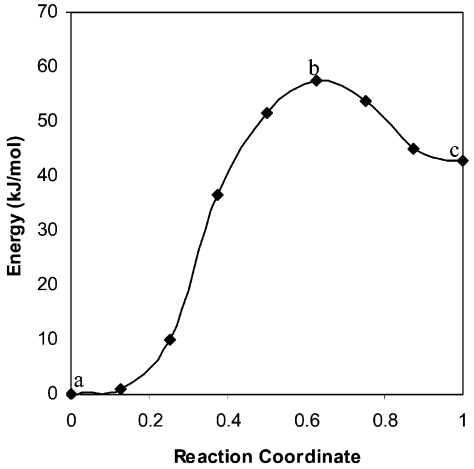

Figure 1. Minimum energy path of the half-self-diffusion of chemisorbed atomic oxygen on Pt(111): O fcc ↔ O hcp.

* To whom all correspondence should be addressed. E-mail: trout@mit.edu.

10.1021/jp048507+ CCC: $27.50
Published on Web 08/05/2004

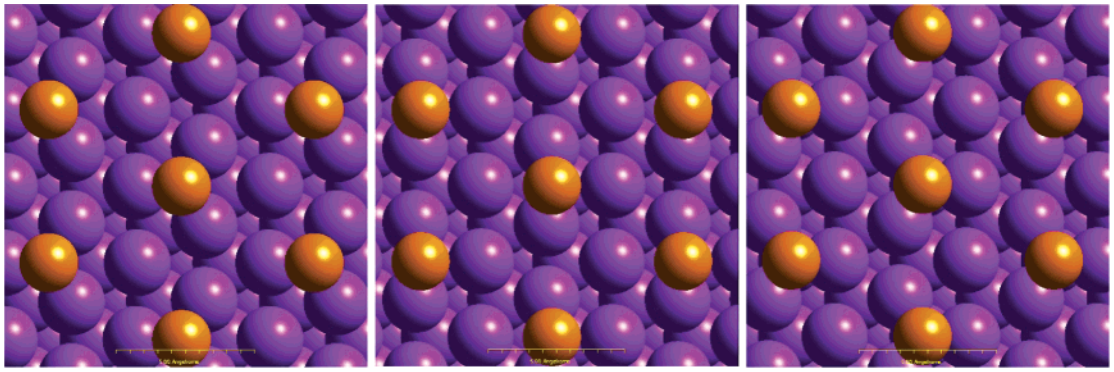

Figure 2. NEB chain images of the half-self-diffusion of chemisorbed atomic oxygen on Pt(111): O fcc ↔ O hcp. Key: (a) O fcc, (b) the transition state, and (c) O hcp.

preferred. The gas-phase oxidation of SO_2 to SO_3 is exothermic but slow in the absence of a catalyst. In this work, we explore two aspects of the oxidation of SO_2 to SO_3 on Pt(111). We first contrast the diffusion kinetics of the three surface species relevant to this chemistry, specifically chemisorbed O, SO_2, and SO_3. Next, drawing on computed thermodynamic data as a guide, we probe the barriers to oxidation of SO_2 to SO_3 starting from the P(2×2)−O covered Pt(111) surface expected to form from saturation exposure to O_2. In particular, we contrast the energetics of Langmuir−Hinshelwood and Eley−Rideal steps in the conversion of SO_2 to SO_3.

II. Computational Details

The GNU publicly licensed software DACAPO[13] was used for the electronic total energy computations. The extended Pt(111) surface was simulated by a three-layer 12-atom slab model with periodic boundary conditions, the accuracy of which was confirmed by a four-layer slab model in computed molecular structures and binding energies.[12] In the direction that is perpendicular to the metal surface plane, a vacuum of ~10 Å was used to separate the slabs. The nonphysical dipole interactions among slabs were annihilated by the self-consistently generated external dipole layer located in the middle of the vacuum. Using this model, a single adsorbate on the surface corresponds to a coverage of $^1/_4$ ML, p(2×2) on Pt(111). The atoms of the bottom layer were fixed at the calculated bulk geometry. The core electrons of all the atoms were treated via the ultrasoft pseudopotentials[14,15] with an energy cutoff of 25 Ry for both the electronic wave function and the density. The d-channel was included explicitly in order to accurately treat the sulfur core.[16] The PW91[17] gradient corrected exchange-correlation functional was used in the self-consistent DFT calculations. Spin polarization effects were not considered to be important and therefore were not treated explicitly for the surface species in the study.

First-principles molecular dynamics have been widely used to study a variety of chemical reactions of insulators and semiconductors that contain finite band-gaps.[18,19] However, a general extension of the Kohn−Sham energy functional[20] to the Mermin free energy functional[21] is needed for the zero-gap metallic systems, making the computations much more complicated.[22,23] Fortunately, many chemical processes on metallic surfaces can be represented accurately by sequences of infrequent transitions from one potential basin to another, the long-time behaviors of which can be treated by transition state theory

TABLE 1: Half of the Symmetric Pathway of the Self-Diffusion of Chemisorbed Atomic Oxygen on Pt(111), O fcc ↔ O hcp, Showing Variation of the Four Pt−O Bond Lengths with Respect to the Self-Diffusion Reaction Coordinate[a]

reaction coordinate	figure index	R_{Pt-O} (Å)				$[^1/_4\sum_{i=1}^4 (R_{Pt-O})_i^2]^{1/2}$
0.000	2a	2.07	2.07	2.07	3.50	2.51
0.125		2.07	2.07	2.08	3.50	2.51
0.250		2.05	2.06	2.17	3.39	2.48
0.375		2.02	2.03	2.53	3.18	2.49
0.500		2.01	2.01	2.80	2.99	2.49
0.625	2b	2.02	2.02	2.73	3.05	2.50
0.750		2.04	2.04	2.40	3.26	2.49
0.875		2.06	2.07	2.17	3.40	2.49
1.000	2c	2.09	2.09	2.09	3.51	2.52
av		2.05	2.05			2.50

[a] Bond lengths are listed in the order of increasing value.

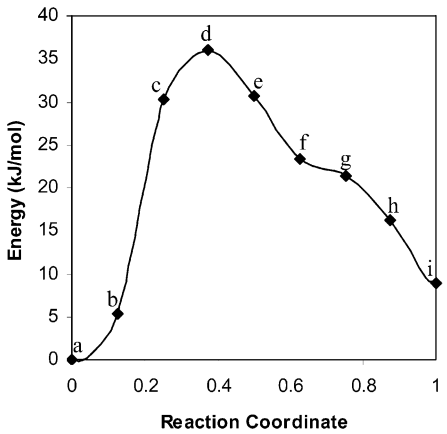

Figure 3. Minimum energy path of the half-self-diffusion of chemisorbed SO_2 on Pt(111) (mechanism I): SO_2 fcc η^2-S_b,O_a ↔ SO_2 hcp η^3-S_a,O_a,O_a.

(TST);[24] i.e., the basin-to-basin transition rate is approximated by the flux through a dividing surface separating the basins.

The nudged elastic band (NEB) method is designed to compute the pathway connecting two local minima, including transition states, by simultaneously relaxing a harmonically connected chain of images that are terminated by the two 3*N* coordinate end points of given reactants and products.[25,26] The reaction pathway is then the series of images between the reactants and products and their energies. For a chemical reaction of given reactants and products, the minimum energy path is found via the NEB method by performing a restrained

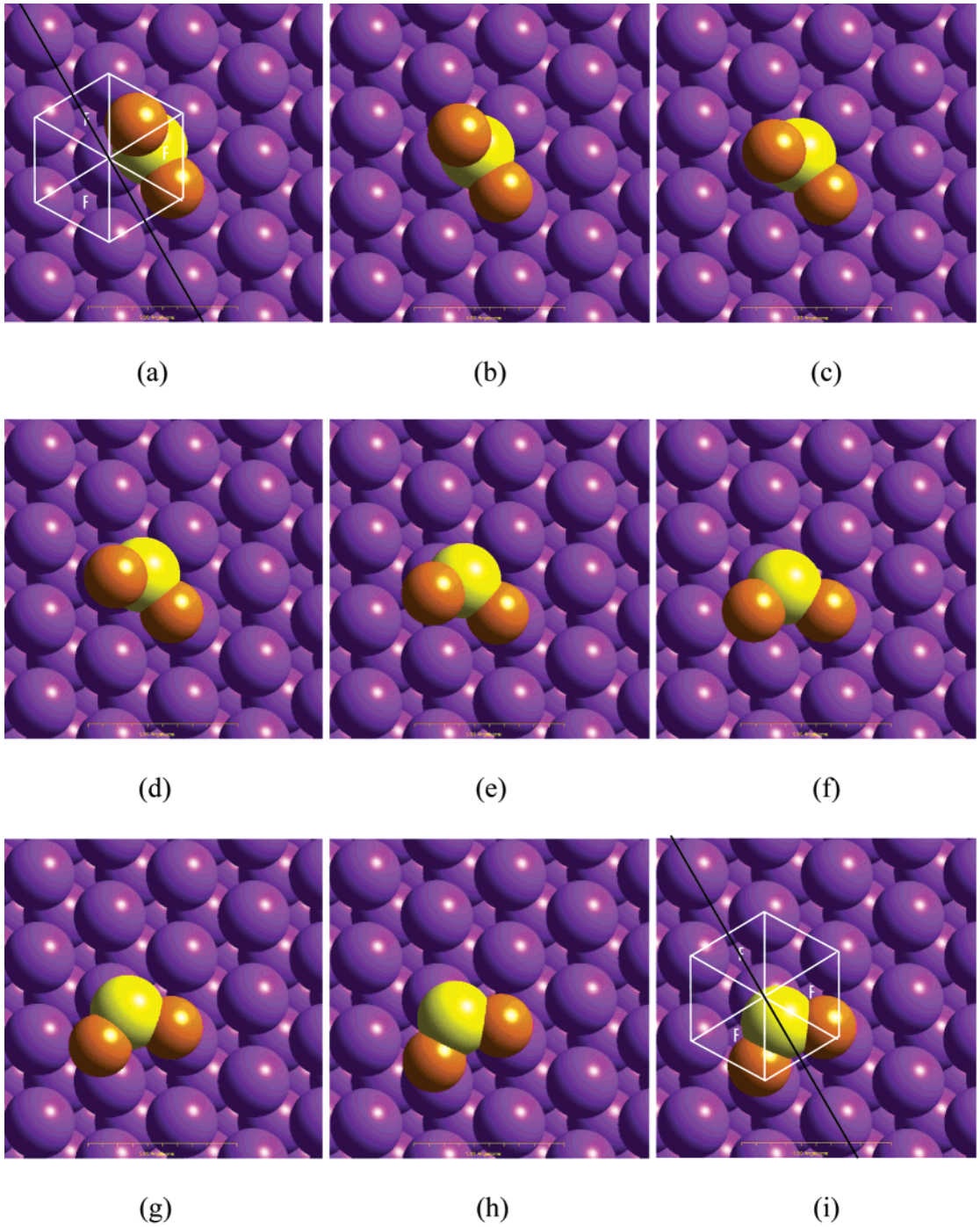

Figure 4. NEB chain images of the half-self-diffusion of chemisorbed SO_2 on Pt(111) (mechanism I): SO_2 fcc η^2-S_b,O_a ↔ SO_2 hcp η^3-S_a,O_a,O_a. Lines are added to frames a and i in order to aid the reader in envisioning the symmetry of the process. The "F"'s mark the fcc sites.

minimization of a series of images on the 3*N*-dimension potential energy surface. The harmonic restraints between adjacent NEB images prevent the collapse of all of the NEB images to the given local minima (namely, the reactants or the products) and ensure that the paths found are indeed the minimum energy paths. The NEB method is particularly useful in combination with planewave DFT computations, since the second- or higher-order derivatives of the Kohn−Sham energy functional with respect to the atomic coordinates are not required. For the relatively simpler self-diffusion computations, identical spring constants connecting all images were chosen, which ensured an equal spacing between adjacent images that span over the activation barrier on the adiabatic potential energy surface. For the more complicated oxidation reaction computations, additional spring constants of double strength were added between images near the transition state regions for better resolution. The locations of these double strength spring constants were determined based on preliminary NEB searches with identical spring constants. The minimization process was terminated when the nudged forces on all images of the chain became small (∼0.07 eV/Å). The highest energy points along the minimum energy paths were considered to be the transition states.

In free energy computations, gas-phase species are treated as ideal, and the transitional, rotational, and vibrational entropies of these species are computed from standard expressions.[27] The harmonic oscillator approximation is used to compute the vibrational entropy contributions to the free energy of the surface

species. Vibrational modes are calculated via diagonalization of the Hessian matrices. Small independent displacements along the Cartesian coordinates were performed, and finite differences of the resulting forces were taken to compute the Hessian matrices. No symmetry was assumed a priori. The equality of the symmetric elements of each Hessian matrix was confirmed. The configurational entropy contributions to the free energy were ignored in this study, to be considered in future studies.[28]

III. Results and Discussion

In this section, we start from the simple case of atomic oxygen diffusion and compare our results to experimental and computational results in the literature. The more complicated case of self-diffusion of SO_2 and SO_3 are examined in sections III.B and III.C. For these two molecular species, the most stable adsorbate location is over an fcc site of the Pt(111) lattice, and similar configurations at an hcp site are slightly (<10 kJ mol^{-1}) higher in energy.[11,12] We thus consider diffusion mechanisms for SO_2 and SO_3 in which they hop from one fcc basin to another via the hcp basins. Because of the symmetry of the adsorbates with respect to the Pt(111) surface at both the fcc and the hcp sites, only half of the self-diffusion reaction pathway, from fcc sites to adjacent hcp sites, is necessary for complete descriptions of these self-diffusion processes. Thus, only half of each of the pathways is presented here. Finally, two possible pathways for conversion of SO_2 to SO_3 are examined in sections III.D and III.E. Summaries of both self-diffusion and overall oxidation reactions are also provided at the ends of section III.C and III.E, respectively.

A. Self-Diffusion of Chemisorbed Atomic O: Mechanism and Analytical Minimum Energy Path. The self-diffusion of chemisorbed atomic oxygen on Pt(111) has been studied both experimentally and computationally.[29−31] A diffusion barrier of 41 kJ mol^{-1} was obtained by Wintterlin et al. in a variable temperature scanning tunneling microscopy (STM) experiment.[29] In addition, several recent DFT studies have shown that the difference in the binding energies of atomic oxygen on fcc sites and hcp sites of Pt(111) is on the order of 39−43 kJ mol^{-1},[31,32] which is the same magnitude as the diffusion barrier of 41 kJ mol^{-1} derived from variable temperature STM. On the basis of these data, it seems that the atomic oxygen on hcp sites is energetically unstable, a conclusion that is inconsistent with the identification of chemisorbed metastable atomic oxygen on hcp sites at 50 K in a recent STM measurement by Stipe et al.[30] Stipe et al. also estimated a lower bound of the diffusion barrier from the hcp sites to the fcc sites to be 12 kJ mol^{-1}. Bogicevic et al.[31] have questioned the accuracy of the low diffusion barrier obtained from the variable temperature STM experiment by Wintterlin et al. and demonstrated that the low barrier of 41 kJ mol^{-1} might be an error associated with conducting the STM measurements within the narrow temperature range of 191−205 K.[31] Bogicevic et al. further concluded that the diffusion energy barrier of atomic oxygen on Pt(111) is ∼56 kJ/mol or ∼53 kJ/mol with a zero-point energy correction included.[31]

From our DFT calculations, atomic oxygen prefers fcc sites at $^1/_4$ ML coverage. The calculated binding energy with respect to atomic O is 411 kJ mol^{-1}, or 43 kJ mol^{-1} greater than the binding energy over hcp sites. These data are also consistent with previous DFT studies, as discussed above.[31,32] In our NEB calculations, the atomic oxygen at these two different 3-fold sites, the fcc and hcp sites, form the reactant and product of the half-self-diffusion process:

$$\text{O fcc} \leftrightarrow \text{O hcp} \qquad \text{(R1)}$$

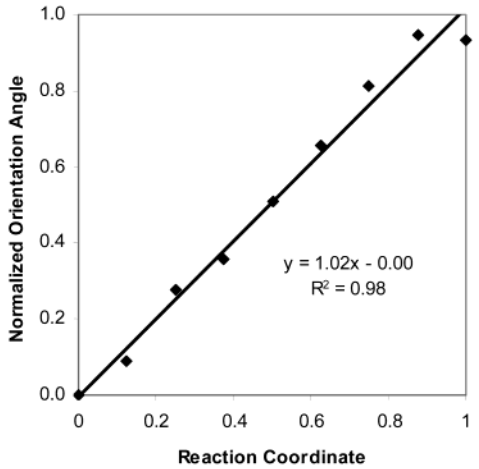

Figure 5. Identification of the reaction coordinate of the half-self-diffusion of chemisorbed SO_2 on Pt(111) (mechanism I): SO_2 fcc η^2-S_b,O_a ↔ SO_2 hcp η^3-S_a,O_a,O_a.

TABLE 2: Half of the Symmetric Pathway of the Self-Diffusion of Chemisorbed SO_2 on Pt(111), SO_2 fcc η^2-S_b,O_a ↔ SO_2 hcp η^3-S_a,O_a,O_a, Showing Variations of Bond Lengths and the SO_2 Molecular Plane Orientation Angle with Respect to the Self-Diffusion Reaction Coordinate[a]

reaction coordinate	figure index	S−O (Å)		Pt−S (Å)		Pt−O (Å)		molecular plane orientation angle (deg)
0.000	4a	1.47	1.53	2.31	2.31	2.30		90
0.125	4b	1.47	1.55	2.30	2.36	2.23		82
0.250	4c	1.48	1.56	2.32	2.63	2.18		65
0.375	4d	1.48	1.57	2.34	2.88	2.16		58
0.500	4e	1.48	1.58	2.38		2.15		44
0.625	4f	1.48	1.57	2.37		2.16		31
0.750	4g	1.49	1.57	2.36		2.17		17
0.875	4h	1.55	1.56	2.31		2.22	2.28	5
1.000	4i	1.55	1.55	2.34		2.24	2.24	6

[a] Bond lengths larger than 3.00 Å are not listed. Listed bond lengths are in the order of increasing value.

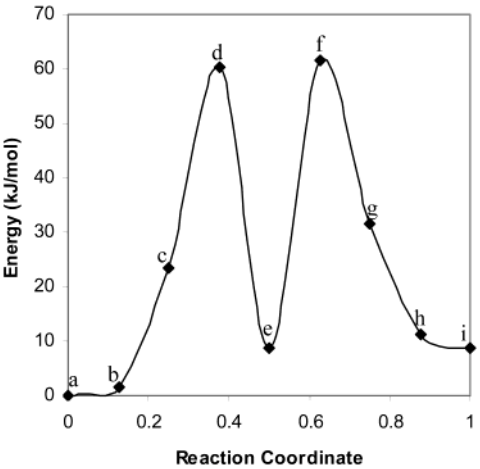

Figure 6. Minimum energy path of the half-self-diffusion of chemisorbed SO_2 on Pt(111) (mechanism II): SO_2 fcc η^2-S_b,O_a ↔ SO_2 bridge η^1-S ⊥ ↔ SO_2 hcp η^2-S_b,O_a.

The minimum energy path of reaction R1 is sketched schematically in Figure 1. The activation energies, without and with zero-point energy corrections, and the activation Gibbs free energy at 600 K and 1 atm are 57, 55, and 59 kJ/mol, respectively. Because the minimum energy path of reaction R1 is relatively straightforward, only the reactant, O fcc, the product, O hcp,

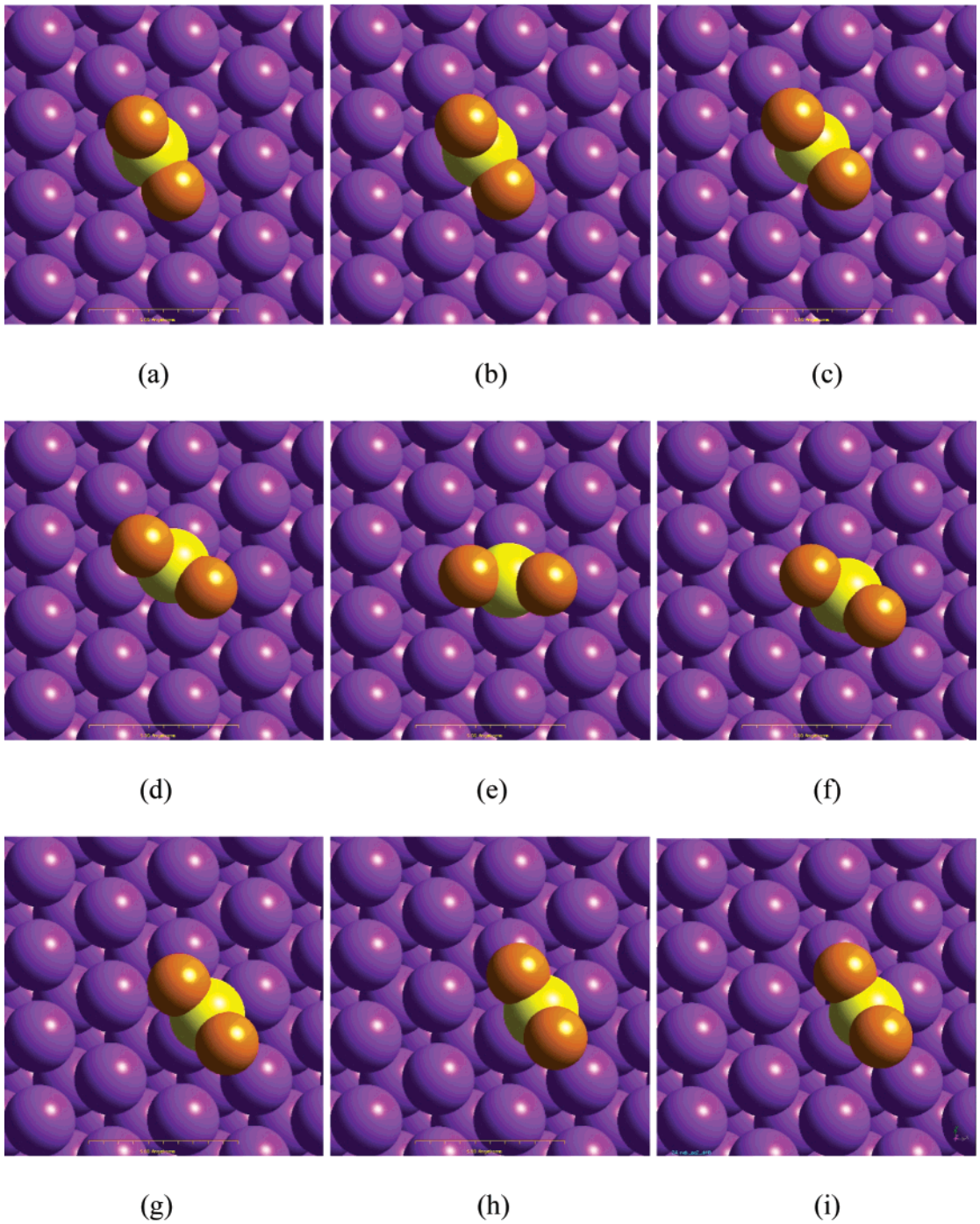

Figure 7. NEB chain images of the half-self-diffusion of chemisorbed SO_2 on Pt(111) (mechanism II): SO_2 fcc η^2-S_b,O_a ↔ SO_2 bridge η^1-S ⊥ ↔ SO_2 hcp η^2-S_b,O_a.

and the transition state are plotted in Figure 2a−c, respectively. Note that the transition state is not exactly over the bridge site, but slightly closer to the hcp site than to the fcc site, as shown in both Figure 1 and Figure 2b, although the difference in energy between the transition state and the point at which the O atom is at the bridge center is small.[31] The shift of the transition state from the exact bridge center toward the energetically less favorable hcp site is consistent with the Hammond postulate.[33]

Taking advantage of the simplicity of the self-diffusion mechanism of chemisorbed atomic oxygen on Pt(111), one can carry out detailed analyses on the representative data points of the minimum energy path in order to gain further understanding of this diffusion process. In the following, we demonstrate how to derive a 3D analytical representation of the minimum energy path for the atomic oxygen self-diffusion process. In particular, one notices that the diffusion path is essentially on the plane that perpendicularly bisects the two bridge atoms. (Refer to Figure 2.) Therefore, the Pt−O bond lengths between the oxygen atom and the two bridge Pt atoms are equal to within a few hundredths of an ångstrom, as listed in the third and forth column in Table 1. Moreover, one notes that the root of the average of the square of the four Pt−O bond length, namely $\sqrt{(^1/_4)\sum_{i=1}^{4}(R_{Pt-O})_i^2}$, is found to be a constant at 2.50 ± 0.01 Å through the whole diffusion reaction path. (Refer to the seventh column of Table 1.) Therefore, when atomic oxygen at $(x,0,z)$ diffuses in the frame of reference of four static metal surface atoms located at $(-\sqrt{3}/2,0,0)$, $(\sqrt{3}/2,0,0)$,

$(0,-1/2,0)$, and $(0,1/2,0)$, the observed constant implies that

$$\left(x+\frac{\sqrt{3}}{2}\right)^2+z^2+\left(x-\frac{\sqrt{3}}{2}\right)^2+z^2+2\times\left(x^2+\left(\frac{1}{2}\right)^2+z^2\right)$$
$$=4\times\left(\frac{2.50}{2.77}\right)^2$$
$$x^2+z^2=0.31\approx\left(\frac{\sqrt{3}}{3}\right)^2$$

i.e., the self-diffusion path is a sector of a circle that connects the fcc site to the hcp site. (Note that all quantities here are in units of the Pt−Pt bond length 2.77 Å in the bulk.)

Certainly, there is a notable physical meaning of such a simple circle-sector representation of the self-diffusion path: it implies that the static close-packed hard-sphere surface atoms and diffusing hard-sphere adsorbates form the essential ingredients of the self-diffusion process of atomic oxygen on the Pt(111) surface. This is a rather surprising result, since both the adsorbate and substrate atoms are subject to full relaxation under the NEB construction. Instead of varying relaxations, however, the substrate Pt atoms relax coherently with respect to the motions of the adsorbate O atom. More importantly, in practice, this implies a universal computational simplification to any substrate and adsorbate systems that satisfies the given hard-sphere conditions, in which we expect that such a circle-sector self-diffusion path is applicable.

B. Self-Diffusion of Chemisorbed SO_2: Pathways and Reaction Coordinates. Although the possible self-diffusion pathways for an atomic species on the Pt(111) surface are limited, the number and complexity of pathways rapidly escalate with the molecularity of the diffusing species. As shown previously,[11] SO_2 can adopt about 20 different stable (or metastable) binding configurations on Pt(111), compared to two in the case of a chemisorbed oxygen atom. For example, both perpendicular and flat-lying configurations of SO_2 on Pt(111) are found to be of comparable energy.[11] Possible self-diffusion hopping processes between any pair of these stable (or metastable) configurations becomes even more complicated, because the number of hopping channels scales quadratically as the number of stable or metastable configurations available. As a reasonable approximation, however, we focus on half-self-diffusion channels from the most energetically stable configuration to other configurations of comparable energy. Two different self-diffusion pathways are considered for the self-diffusion of chemisorbed SO_2 on Pt(111). The first pathway is

$$SO_2\ \text{fcc}\ \eta^2\text{-}S_b,O_a \leftrightarrow SO_2\ \text{hcp}\ \eta^3\text{-}S_a,O_a,O_a \qquad \text{(R2)}$$

Note that a special nomenclature is used here. First, fcc or hcp indicates that the adsorbate SO_2 molecule sits primarily above an fcc site or an hcp site on the Pt(111) surface, respectively. η^n indicates that there are n atoms directly bound to the surface. Following the dash are the names of the atoms that are directly bound to the surface. Subscripts indicate the exact binding site of the corresponding atoms, where a stands for atop, b stands for bridge, f stands for fcc, and h stands for hcp. One may refer to our previous work for more details of this nomenclature.[11] The minimum energy path of reaction R2 is plotted in Figure 3. As shown, the activation energy of the diffusion reaction of molecular SO_2 from the bicoordinated configuration at fcc sites, SO_2 fcc η^2-S_b,O_a, to the tri-coordinated configuration at hcp sites, SO_2 hcp η^3-S_a,O_a,O_a, is 36 kJ/mol. The activation energy increases to 42 kJ/mol after the zero-point energy correction, and the activation Gibbs free energy is estimated to be 47 kJ/mol at 600 K and 1 atm.

TABLE 3: Half of the Symmetric Pathway of the Self-diffusion of Chemisorbed SO_2 on Pt(111), SO_2 fcc η^2-S_b,O_a ↔ SO_2 Bridge η^1-S ⊥ ↔ SO_2 hcp η^2-S_b,O_a, Showing Variations of Bond Lengths and the Perpendicular SO_2 Molecular Plane Rotation Angle with Respect to the Self-Diffusion Reaction Coordinate[a]

reaction coordinate	figure index	S−O (Å)		Pt−S (Å)		Pt−O (Å)	perpendicular molecular plane rotation angle (deg)
0.000	7a	1.47	1.53	2.31	2.31	2.30	38
0.125	7b	1.47	1.53	2.31	2.32	2.33	45
0.250	7c	1.47	1.49	2.31	2.46	2.82	40
0.375	7d	1.47	1.48	2.29	2.94		57
0.500	7e	1.48	1.48	2.35	2.35		90
0.625	7f	1.47	1.48	2.32	2.97		58
0.750	7g	1.47	1.49	2.31	2.55	2.97	41
0.875	7h	1.47	1.51	2.33	2.35	2.54	32
1.000	7i	1.47	1.52	2.32	2.33	2.43	30

[a] Bond lengths larger than 3.00 Å are not listed. Listed bond lengths are in the order of increasing value.

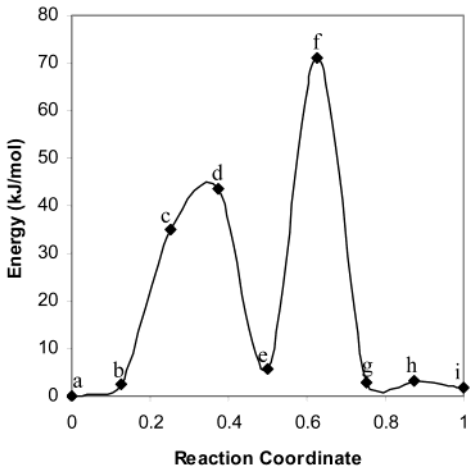

Figure 8. Minimum energy path of half-self-diffusion of chemisorbed SO_3 on Pt(111): SO_3 fcc η^2-S_a,O_a,O_a ↔ SO_3 hcp η^3-S_a,O_a,O_a $\xleftrightarrow{60^\circ}$ SO_3 hcp η^3-S_a,O_a,O_a.

All of the NEB chain images, including the reactant, product, and seven intermediate representative points are plotted in Figure 4. Note that in Figure 4, images a and i, lines are added to aid the reader in visualizing the symmetries of the adsorbates with respect to the surface as described at the beginning of this section. Interestingly, it is found that the orientation angle between the SO_2 molecular plane and the metal surface plane is the genuine reaction coordinate of the diffusion mechanism (reaction R2), as demonstrated by the linear dependence between the normalized orientation angle and the calculated reaction coordinate, as shown in Figure 5. The normalized orientation angle is defined as the normalization value of the SO_2 molecular plane orientation angle (in the angle range of [90°, 0°]) with respect to the metal surface plane, as listed in the last column of Table 2.

The second pathway for chemisorbed SO_2 half-self-diffusion that we investigated involves two intermediate steps

$$SO_2\ \text{fcc}\ \eta^2\text{-}S_b,O_a \leftrightarrow SO_2\ \text{bridge}\ \eta^1\text{-S}\perp \leftrightarrow SO_2\ \text{hcp}\ \eta^2\text{-}S_b,O_a \qquad \text{(R3)}$$

Here bridge indicates that the chemisorbed SO_2 is primarily over a bridge site and ⊥ indicates that the SO_2 molecular plane is

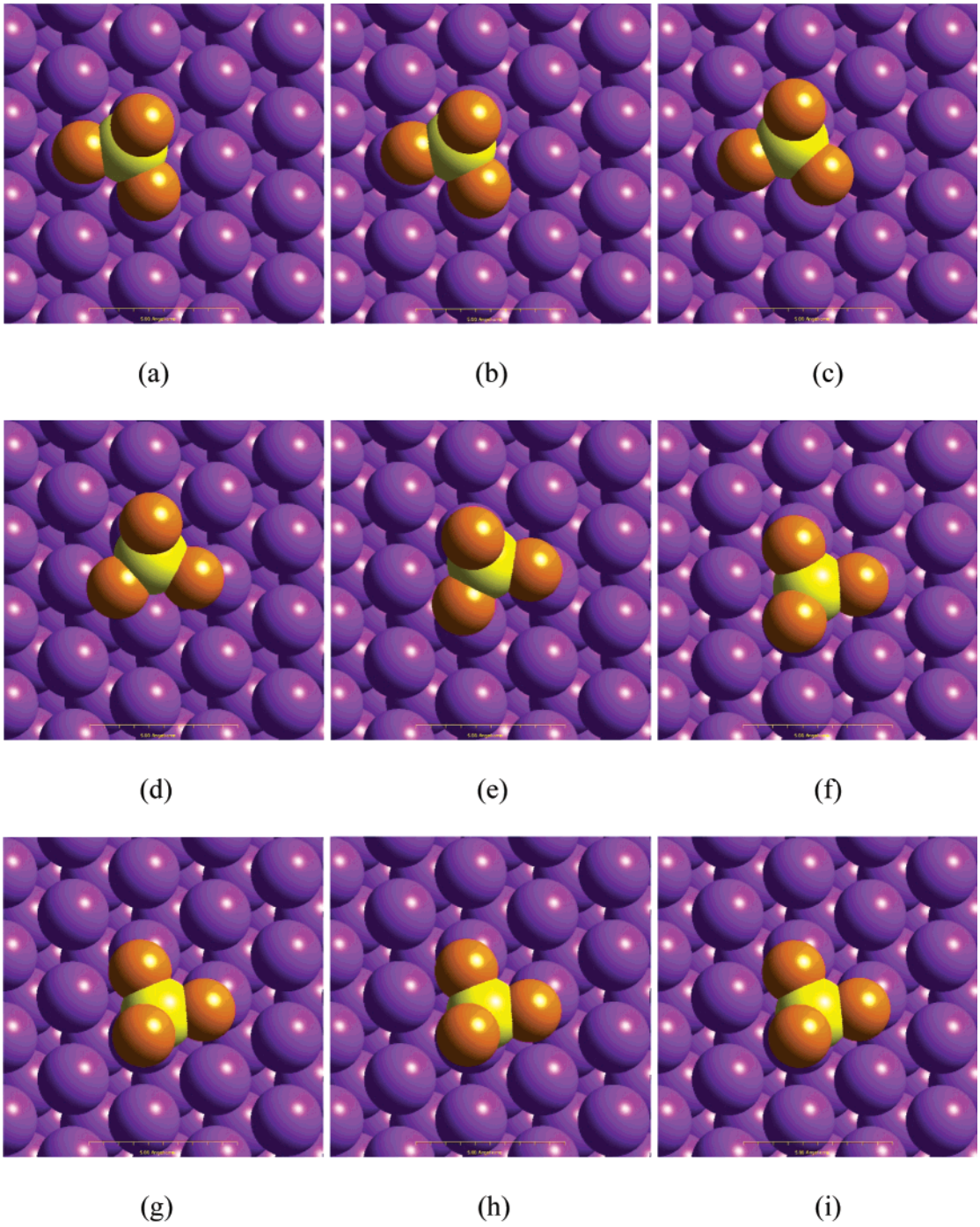

Figure 9. NEB chain images of the half-self-diffusion of chemisorbed SO_3 on Pt(111): SO_3 fcc η^2-S_a,O_a,O_a ↔ SO_3 hcp η^3-S_a,O_a,O_a $\overset{60°}{\longleftrightarrow}$ SO_3 hcp η^3-S_a,O_a,O_a.

perpendicular to the line connecting the two bridge Pt atoms.[11] As shown in Figure 6, the two activation energy barriers, corresponding to the first and second points of (R3), are of the same order of magnitude: the second barrier is 62 kJ/mol, about 2 kJ/mol higher than the first barrier and about 26 kJ/mol higher than the barrier of the first diffusion mechanism (reaction R2). Therefore, we conclude that reaction R2 is more likely to contribute to the self-diffusion of SO_2 on the Pt(111) surface.

Interestingly, the matrix elements that describe the rotation of the plane of SO_2 with respect to the plane of the surface in the reaction coordinates of the first and the second mechanisms are orthogonal. In particular, the SO_2 molecular plane orientation angle, which is parallel to the reaction coordinate of the first mechanism (Figure 5), turns out to be constant at 90° in the second mechanism. Thus, in reaction R3, the SO_2 molecular plane is always perpendicular to the metal surface, as shown in the NEB chain image plot of Figure 7, parts a−i. Nevertheless, the angle of the perpendicular SO_2 molecular plane with respect to the two bridge Pt atoms between the fcc and hcp sites, as listed in the last column of Table 3, is virtually a monotonic function of the reaction coordinate of the second mechanism. The deviation from the linear dependence relation is mainly because the surface electron density is not evenly distributed along the angular direction. A similar effect of the uneven distribution of electron density causes the small deviation of the proportional relation shown in Figure 5, when the SO_2 molecular plane is close to the flat-lying configuration.

TABLE 4: Half of the Symmetric Pathway of the Self-Diffusion of Chemisorbed SO_3 on Pt(111), SO_3 fcc η^2-S_a,O_a,O_a ↔ SO_3 hcp η^3-S_a,O_a,O_a $\overset{60°}{\longleftrightarrow}$ SO_3 hcp η^3-S_a,O_a,O_a, Showing Variation of Bond Lengths with Respective to the Self-Diffusion Reaction Coordinate

reaction coordinate	figure index	S−O (Å)			Pt−S (Å)		Pt−O (Å)	
0.000	9a	1.46	1.56	1.56	2.31		2.16	2.16
0.125	9b	1.46	1.56	1.57	2.31		2.15	2.18
0.250	9c	1.46	1.53	1.56	2.29		2.20	2.52
0.375	9d	1.47	1.52	1.56	2.29		2.27	2.67
0.500	9e	1.46	1.53	1.56	2.31		2.15	2.37
0.625	9f	1.46	1.53	1.55	2.40	2.78	2.18	2.30
0.750	9g	1.46	1.54	1.57	2.31		2.29	2.14
0.875	9h	1.46	1.55	1.56	2.30		2.16	2.22
1.000	9i	1.46	1.56	1.56	2.31		2.18	2.18

[a] Bond lengths larger than 2.80 Å are not listed. Listed bond lengths are in the increasing order.

In summary, we have identified two complementary pathways for the self-diffusion of chemisorbed SO_2 on the Pt(111) surface. The more favorable pathway has an activation energy of 42 kJ/mol at 0 K and an activation free energy of 47 kJ/mol at 600 K and 1atm.

C. Self-Diffusion Pathway for Chemisorbed SO_3. The minimum energy path for the half-self-diffusion of chemisorbed SO_3 on Pt(111) is shown in Figure 8, where

$$SO_3 \text{ fcc } \eta^2\text{-}S_a,O_a,O_a \leftrightarrow SO_3 \text{ hcp } \eta^3\text{-}S_a,O_a,O_a \overset{60°}{\longleftrightarrow} SO_3 \text{ hcp } \eta^3\text{-}S_a,O_a,O_a \quad \text{(R4)}$$

The activation energy of 71 kJ/mol is obtained from the barrier height of the second step of reaction R4. A smaller barrier height of 43 kJ/mol is obtained for the first step of reaction R4. The overall activation energy decreases to 68 kJ/mol after the zero-point energy correction, and the activation Gibbs free energy is estimated to be 64 kJ/mol at 600 K and 1 atm.

Similar to reaction R3, the reaction mechanism of the first step of reaction R4 involves a rotational motion that shifts the SO_3 molecule from the fcc site (Figure 9a), via the bridge site transition state (Figure 9d), to the hcp site (Figure 9e). The overall geometry of the adsorbates does not experience any major changes; for example, the three S−O bond lengths vary only a few percent of an ångstrom during the rotation process. On the other hand, the sharing of surface metal atoms among the adsorbate atoms at the transition state (Figure 9d) causes the energy of adsorption of the molecule to be small.[11] The sharing of surface metal atoms is also responsible for the large increases in the Pt−O bond length, by ∼0.1−0.5 Å, due to the fact that Pt−S bonds are stronger than Pt−O bonds.[11] (Refer to Table 4 for details.)

A simple rotational motion, however, cannot by itself be the governing reaction coordinates for these diffusion processes. Certain shifts in the rotation axes are needed to be coupled to the rotation motions. For example, the diffusion mechanism of reaction R3 requires two different rotation axes, one at the fcc site of the first step and the other at the hcp site of the second step. (Refer to Figure 7.) Nevertheless, the second step of reaction R4, the apparent 60° pure rotation within the hcp site, turns out to follow a surprisingly different course, flipping to switch between two tetrahedral binding configurations (Figure 9e,i) via a planar intermediate (Figure 9f). Note that this is somewhat surprising, because the symmetry of the planar intermediate is similar to that of the stable gas-phase SO_3, surface SO_3 species generally prefer tetrahedral type of bindings.[12] Note that this planar intermediate (Figure 9f) has the largest first-neighbor Pt−S bond, 2.40 Å, as shown in Table 4. Stretching the Pt−S bond is generally indicative of a significant decrease in stabilization.[11]

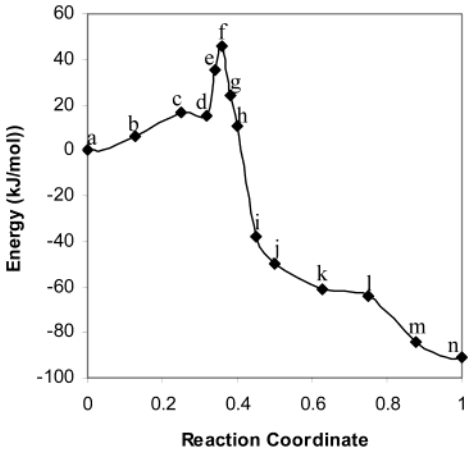

Figure 10. Minimum energy path of the oxidation of SO_2 on Pt(111) (Langmuir−Hinshelwood mechanism): O fcc + SO_2 fcc η^2-S_b,O_a ↔ SO_3 fcc η^3-S_a,O_a,O_a.

In summary, very different self-diffusion pathways exist for surface O, SO_2 and SO_3 species on the Pt(111) surface. In the simplest case, we have found a simple analytical expression for the reaction coordinate of the atomic O self-diffusion minimum energy path. Taking advantage of the well-defined molecular plane of SO_2, we have identified two different reaction mechanisms. One of these helps to explain the first step of the diffusion pathway examined for SO_3. It is also interesting that the barrier to diffusion of SO_2 is much less than that of SO_3, 36 vs 71 kJ/mol, even though their energies of adsorption do not differ much, 98 vs 113 kJ/mol.[11,12] Also, we note that while we have chosen as our end points in the NEB calculations the most stable adsorbed configurations for both SO_2 and SO_3, it is possible, although unlikely, that less stable adsorption configurations could have substantially lower barriers, leading to alternate pathways. On the basis of our results, the barrier for diffusion decreases in the following order on the Pt(111) surface: molecular SO_2, atomic O, and molecular SO_3.

D. Oxidation of SO_2: Langmuir—Hinshelwood Surface Reaction Step. In this section and the next one, we present results on two of the surface reactions for the oxidation of SO_2 to SO_3 on the Pt(111). The first one occurs between SO_2 and an O atom, both adsorbed together in a p(2×2) configuration. We call this the Langmuir−Hinshelwood surface reaction step. The second one occurs between a gas-phase SO_2 molecule and an absorbed O atom in a p(2×2) configuration. We call this a Eley−Rideal surface reaction step. The energies and reaction pathways of each are discussed and compared. For the Langmuir−Hinshelwood surface reaction step, we consider the following reaction:

$$O \text{ fcc} + SO_2 \text{ fcc } \eta^2\text{-}S_b,O_a \leftrightarrow SO_3 \text{ fcc } \eta^3\text{-}S_a,O_a,O_a \quad \text{(R5)}$$

Note that the reactant of reaction R5 is obtained by adding an SO_2 fcc η^2-S_b,O_a molecule to the P(2×2)−O fcc supercell, followed by a geometry optimization. The calculated minimum energy path of reaction R5 is plotted schematically in Figure 10. As shown, the activation energy is 46 kJ/mol or 42 kJ/mol with the zero-point energy corrections. The activation Gibbs free energy is 45 kJ/mol at 600 K and 1 atm.

The reactant, 12 intermediate NEB images, and the product are shown in Figure 11a−n. As shown in Table 5, the S−O_a

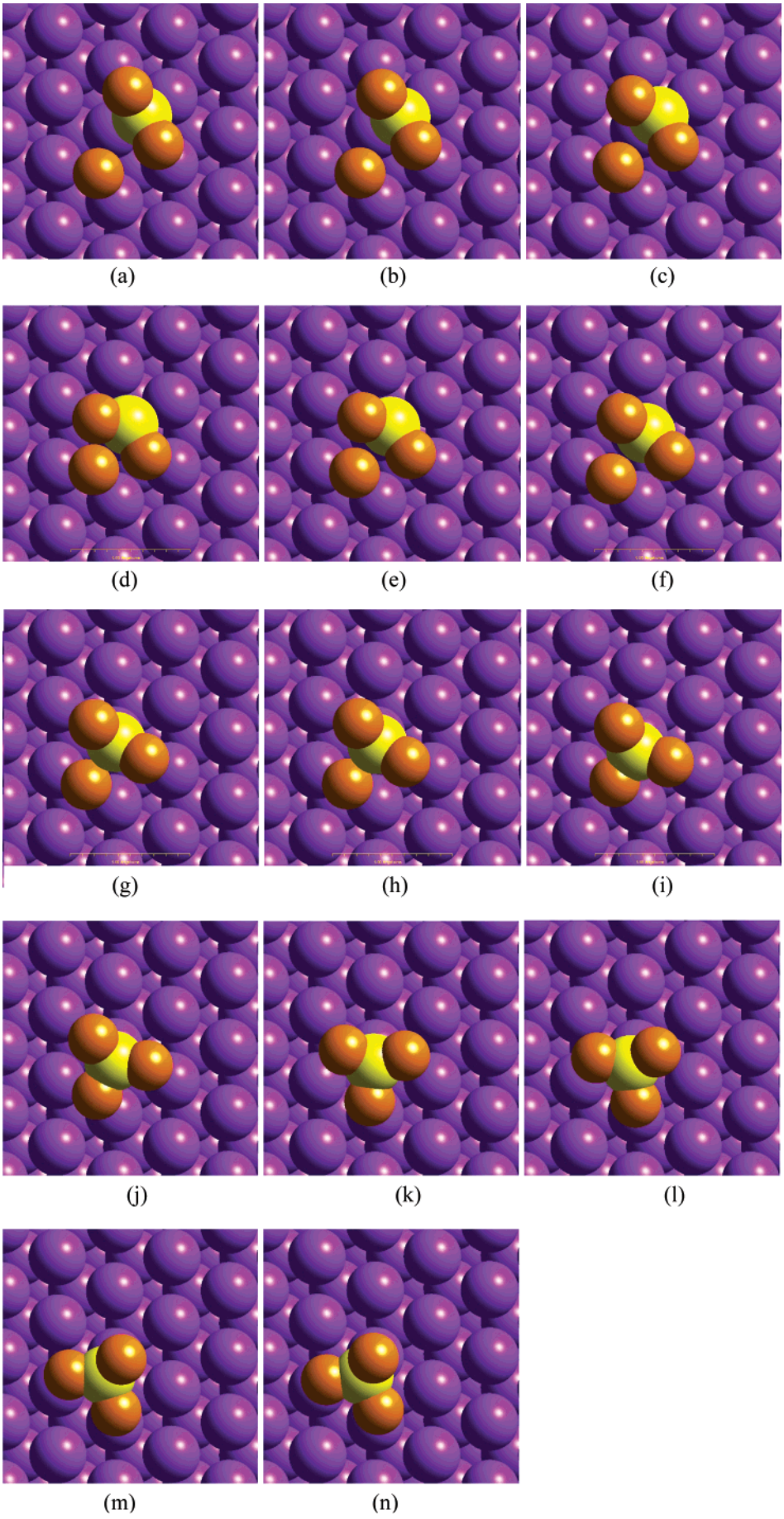

Figure 11. NEB chain images of the oxidation of SO_2 on Pt(111) (Langmuir−Hinshelwood mechanism): O fcc + SO_2 fcc η^2-S_b,O_a ↔ SO_3 fcc η^3-S_a,O_a,O_a.

TABLE 5: Oxidation Reaction of SO_2 on Pt(111), Showing Variation of the Distance between the Sulfur Atom and the Preadsorbed Oxygen Atom with Respect to the Self-Diffusion Reaction Coordinate[a]

figure index (L−H)	11a	11b	11c	11d	11e	11f	11g	11h	11i
energy (kJ/mol) (L−H)	0	6	17	15	35	46	24	11	−38
S−O_a (Å) (L−H)	3.19	3.05	3.00	2.83	2.76	2.61	2.36	2.15	1.80
figure index (L−H)	11j	11k	11l	11m	11n				
energy (kJ/mol) (L−H)	−50	−61	−64	−84	−91				
S−O_a (Å) (L−H)	1.60	1.60	1.58	1.57	1.56				
figure index (E−R)	14a	14b	14c	14d	14e	14f	14g	14h	14i
energy (kJ/mol) (E−R)	0	1	3	−1	−1	3	21	25	12
S−O_a (Å) (E−R)	2.38	2.37	2.37	2.36	2.35	2.34	2.26	2.18	1.90
figure index (E−R)	14j	14k	14l	14m	14n	14o			
energy (kJ/mol) (E−R)	6	−3	−25	−62	−78	−95			
S−O_a (Å) (E−R)	1.75	1.56	1.47	1.58	1.57	1.57			

[a] L−H and E−R stand for the Langmuir−Hinshelwood mechanism and the Eley-Rideal mechanism, respectively.

TABLE 6: Summary of Activation Energies, Where L−H and E−R Stand for the Langmuir−Hinshelwood Mechanism and the Eley−Rideal Mechanism, Respectively

reaction	E_a (kJ/mol)	E_a with the zero-point energy correction (kJ/mol)	G_a at 600 K and 1 atm (kJ/mol)
O self-diffusion (reaction R1)	57	55	59
SO_2 half-self-diffusion (reaction R2)	36	42	47
SO_3 half-self-diffusion (reaction R4)	71	68	64
SO_2 oxidation (L−H) (reaction R5c′)	46	42	45
SO_2 oxidation (E−R) (reaction R6c′)	25	24	26

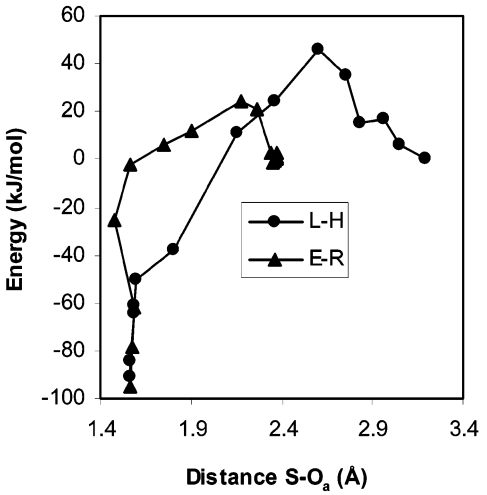

Figure 12. Projection of the minimum energy paths of the oxidations of SO_2 on Pt(111) on the S−O_a bond direction. H−L and E−R represent the Langmuir−Hinshelwood mechanism and Eley−Rideal mechanisms, respectively.

distance, namely, the distance between the sulfur atom of the SO_2 molecule and that of the preadsorbed oxygen, is a monotonic function of the reaction coordinate obtained from the NEB calculations. However, as clearly illustrated in Figure 12, the reaction coordinate is more complex than merely the S−O_a distance, starting roughly as the separation vector of S−O_a mixed with the SO_2 out-of-plane deforming vibrational motion, and ending as a rotational motion with respect to the C_{3v} axis of the molecular SO_3. A projection of the minimum energy path onto the one-dimensional S−O_a bond direction is plotted in Figure 12. The steep ascent (rather than the slow ascent) of the energy value with respect to the increase of the S−O_a bond length at ∼1.56 Å confirms that the actual reaction coordinate is essentially orthogonal to the S−O_a bond direction as the molecular is being formed.

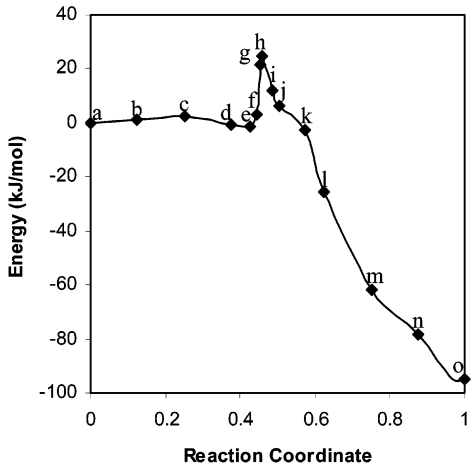

Figure 13. Minimum energy path of the oxidation of SO_2 on Pt(111) (Eley−Rideal mechanism): (SO_2 (g) + O fcc) ↔ SO_3 fcc η^3-S_a,O_a,O_a.

E. Oxidation of SO_2: Eley—Rideal Surface Reaction Step. In the Eley−Rideal surface reaction step studied using our model, the gas-phase SO_2 molecule first preadsorbs on an O atom in a p(2×2) supercell:

$$SO_2(g) + O(a) \leftrightarrow (SO_2(g) + O(a)) \quad \Delta E = -6.9 \text{ kJ/mol} \qquad \text{(R6a)}$$

Next, this system reacts to form adsorbed SO_3.

$$(SO_2\ (g) + O\ fcc) \leftrightarrow SO_3\ fcc\ \eta^3\text{-}S_a,O_a,O_a \qquad \text{(R6b)}$$

We calculated the barrier for reaction R6b to be 25 kJ/mol, as shown in Figure 13. When a common reference state, such as the identical product of SO_3 fcc η^3-S_a,O_a,O_a of both reactions R5 and R6b, is chosen, the barrier of the Eley−Rideal surface reaction step (Figure 14e) is lower than that of the Langmuir−Hinshelwood surface reaction step (Figure 11d) by 17 kJ/mol.

Compared to the Langmuir−Hinshelwood surface reaction step of reaction R5, the reaction coordinate of the Eley−Rideal surface reaction step of reaction R6b does not correlate well with the S−O_a bond direction, as shown in Figure 12. However, both elementary reactions exhibit rotational motion with respect to the C_{3v} axis of SO_3 as molecular SO_3 is formed. This motion results from the tetrahedral bonding to the metal surface. On the other hand, the flipping process occurs in reaction R6b as well, similar to the mechanism in the second diffusion step of the self-diffusion reaction of SO_3. The difference is that the molecular plane of planar SO_3 is almost perpendicular to the metal surface in the former case (Figure 14f), but the molecular plane of SO_3 is almost parallel to the metal surface in the latter case (Figure 9f). Moreover, as illustrated in Figure 14a−c, the

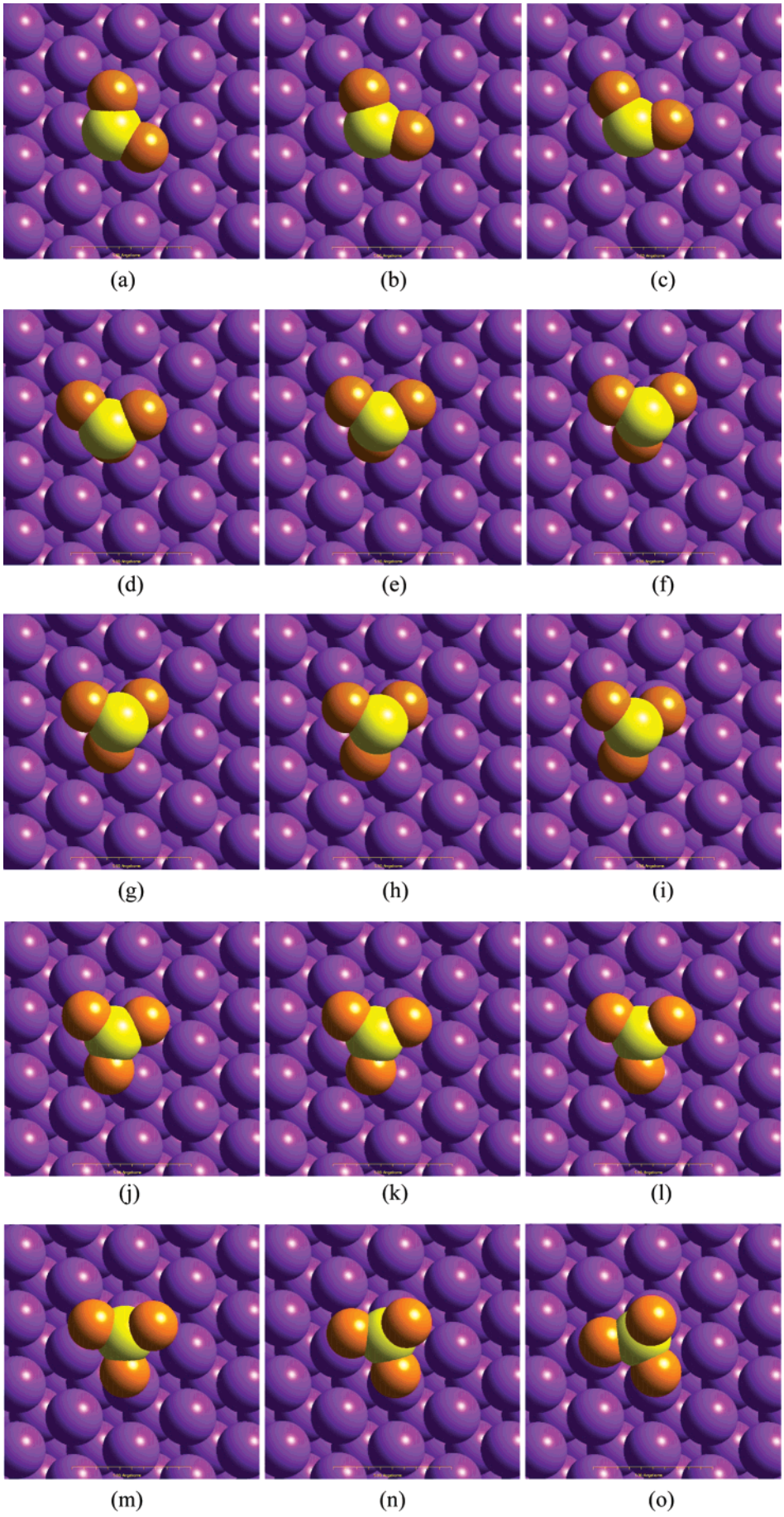

Figure 14. NEB chain images of the oxidation of SO_2 on Pt(111) (Eley−Rideal mechanism): (SO_2 (g) + O fcc) ↔ SO_3 fcc η^3-S_a,O_a,O_a.

rotational motion of the gas-phase SO_2 molecule with respect to its perpendicular axis occurs at the beginning of the Eley−Rideal surface reaction step, which terminates at the point where the gas-phase SO_2 interacts with the favorable distribution of the surface electron density and rapidly connects to the preadsorbed surface oxygen atom.

In summary, our first-principles DFT calculations demonstrate that for the catalytic oxidation of SO_2 to SO_3 on the p(2×2)−O precovered Pt(111) surface, the barrier for the Eley−Rideal surface reaction step is significantly less than that for the Langmuir−Hinshelwood surface reaction step (Table 6). This is mainly due to the fact that the Langmuir−Hinshelwood surface reaction step involves a more constrained transition state (Figure 11f). In other words, it is easier for molecular SO_2 to move to the top of the chemisorbed oxygen atom from the gas phase than to move across the Pt surface, dragging substrate Pt atoms together.

IV. Conclusions

We have performed DFT-GGA calculations with the objective of investigating several important steps in the Pt(111)-catalyzed oxidation of SO_2 to SO_3 on the Pt(111) surface. As found previously,[31] O atoms diffuse via jumps between fcc and hcp hollows on the Pt(111) surface with an activation barrier of 57 kJ mol^{-1}. Similar fcc to hcp diffusion pathways for SO_2 and SO_3 have been identified: SO_2 can diffuse with a somewhat lower activation energy than O, reflecting the variety of comparably bound hollow and bridge configurations available to SO_2 on the Pt(111) surface;[11] the activation energy for SO_3 diffusion is greater than that for O, reflecting the more pronounced preference for SO_3 to bind directly over fcc and hcp sites.[12] Within the supercell model employed here, two pathways are identified for the combination of SO_2 and O to form SO_3. Preadsorption of SO_2 on Pt(111) before reaction, as would be expected for a standard Langmuir−Hinshelwood surface reaction step, leads to a transition state with somewhat higher energy than direct reaction of SO_2 from the gas phase with surface-bound O, a standard Eley−Rideal surface reaction step. The results are consistent with the ready conversion of SO_2 to SO_3 observed over Pt catalysts and suggest that this oxidation could have a significant contribution from an Eley−Rideal type pathway. Because of the large sensitivity of the surface thermodynamics to oxygen-coverage previously found for SO_x on Pt,[12] as well as the stability of surface-bound SO_4 under highly oxidizing conditions, the actual mechanism of sulfur oxidation is likely to be highly sensitive to environmental conditions. The results of this and previous studies are currently being used in more course-grained simulations to examine the effects of different environmental conditions in more detail.

Acknowledgment. This work was supported by the Ford Motor Company and the National Science Foundation, CTS-9984301.

References and Notes

(1) Ceyer, S. T. *Annu. Rev. Phys. Chem.* **1988**, *39*, 479.

(2) *Surface Science, The First Thirty Years*; Duke, C. B., Ed.; North-Holland: Amsterdam, 1994.

(3) Hamers, R. J. *J. Phys. Chem.* **1996**, *100*, 13103.

(4) Radeke, M. R.; Carter, E. A. *Annu. Rev. Phys. Chem.* **1997**, *48*, 243.

(5) Gro*β*, A. *Surf. Sci. Rep.* **1998**, *32*, 291.

(6) Taylor, K. C. Automobile Catalytic Converters. In *Catalysis Science and Technology*; Anderson, J. R., Boudart, M., Eds.; Springer-Verlag: Berlin, 1984; Vol. 5; p 119.

(7) Rodriguez, J. A.; Hrbek, J. *Acc. Chem. Res.* **1999**, *32*, 719.

(8) Haase, J. *J. Phys.: Condens. Matter* **1997**, *9*, 3647.

(9) Shelef, M.; McCabe, R. W. *Catal. Today* **2000**, *62*, 35.

(10) Rodriguez, J. A.; Ricart, J. M.; Clotet, A.; Illas, F. *J. Chem. Phys.* **2001**, *115*, 454.

(11) Lin, X.; Hass, K. C.; Schneider, W. F.; Trout, B. L. *J. Phys. Chem. B* **2002**, *106*, 12575.

(12) Lin, X.; Schneider, W. F.; Trout, B. L. *J. Phys. Chem. B* **2004**, *108*, 250.

(13) http://www.fysik.dtu.dk/CAMP/dacapo.html.

(14) Vanderbilt, D. *Phys. Rev. B* **1990**, *41*, 7892.

(15) Laasonen, K.; Pasquarello, A.; Car, R.; Lee, C.; Vanderbilt, D. *Phys. Rev. B* **1993**, *47*, 10142.

(16) Lin, X.; Ramer, N. J.; Rappe, A. M.; Hass, K. C.; Schneider, W. F.; Trout, B. L. *J. Phys. Chem. B* **2001**, *105*, 7739.

(17) Perdew, J. P.; Chevary, J. A.; Vosko, S. H.; Jackson, K. A.; Pederson, M. R.; Singh, D. J.; Fiolhais, C. *Phys. Rev. B* **1992**, *46*, 6671.

(18) Car, R.; Parrinello, M. *Phys. Rev. Lett.* **1985**, *55*, 2471.

(19) Marx, D.; Hutter, J. Ab initio molecular dynamics: Theory and Implementation. In *Modern Methods and Algorithms of Quantum Chemistry*; Grotendorst, J., Ed.; John von Neumann Institute for Computing: Jülich, Germany, 2000; Vol. 1; p 301.

(20) Kohn, W.; Sham, L. J. *Phys. Rev.* **1965**, *140*, A1133.

(21) Mermin, N. D. *Phys. Rev.* **1964**, *137*, A1441.

(22) Alavi, A.; Kohanoff, J.; Parrinello, M.; Frenkel, D. *Phys. Rev. Lett.* **1994**, *73*, 2599.

(23) Marzari, N.; Vanderbilt, D.; Payne, M. C. *Phys. Rev. Lett.* **1997**, *79*, 1337.

(24) Truhlar, D. G.; Garrett, B. C.; Klippenstein, S. J. *J. Phys. Chem.* **1996**, *100*, 12771.

(25) Henkelman, G.; Johannesson, G.; Jónsson, H. Methods for Finding Saddle Points and Minimum Energy Paths. In *Progress on Theoretical Chemistry*; Schwartz, S. D., Ed.; Kluwar Academic Publishers: Dordrecht, The Netherlands, 2000; p 269.

(26) Jonsson, H.; Mills, G.; Jacobsen, K. W. Nudged Elastic Band Method for Finding Minimum Energy Paths of Transitions. In *Classical and Quantum Dynamics in Condensed Phase Simulations*; Berne, B. J., Ed.; World Scientific: Singapore, 1998; p 385.

(27) McQuarrie, D. A. *Statitistical Mechanics*; Harper Collins Publishers: New York, 1976.

(28) Tang, H.; Van der Ven, A.; Trout, B. L. *Phys. Rev. B* **2004**, 045420.

(29) Wintterlin, J.; Schuster, R.; Ertl, G. *Phys. Rev. Lett.* **1996**, *77*, 123.

(30) Stipe, B. C.; Rezaei, M. A.; Ho, W.; Gao, S.; Persson, M.; Lundqvist, B. I. *Phys. Rev. Lett.* **1997**, *78*, 4410.

(31) Bogicevic, A.; Strömquist, J.; Lundqvist, B. I. *Phys. Rev. B* **1998**, *57*, R4289.

(32) Feibelman, P. J.; Esch, S.; Michely, T. *Phys. Rev. Lett.* **1996**, *77*, 2257.

(33) Hammond, G. S. *J. Am. Chem. Soc.* **1955**, *77*, 334.